

A State Space Approach for the Analysis of Doubly Curved Functionally Graded Elastic and Piezoelectric Shells

Chih-Ping Wu^{1,2} and Kuo-Yen Liu²

Abstract: Based on the three-dimensional (3D) piezoelectricity, we present the exact solutions of simply-supported, doubly curved functionally graded (FG) elastic and piezoelectric shells using a state space approach. A set of the dimensionless coordinates and field variables is introduced in the present formulation to prevent from the ill-conditioned problem in the relevant computation. By means of direct elimination, we reduce the twenty-two basic differential equations to a set of eight state variable equations (or state equations) with variable coefficients of the thickness coordinate. By means of the successive approximation method, we artificially divide the shell into a NL -layered shell and the thickness of each layer is small. That leads to a reasonable manipulation to reduce the state equations of a thickness-varying system for each individual layer to those of a thickness-invariant system. Imposition of the boundary conditions on the lateral surfaces of the shell, the state variables through the thickness coordinate can then be determined using the method of propagator matrix. The direct and converse effects on the static behavior of doubly curved, multilayered and FG piezoelectric shells are studied. The accuracy and the rate of convergence of the present state space approach are evaluated.

Keyword: Piezoelectric material, Shells, 3D solutions, FG material; Static, Electro-elastic analysis; A state space approach

1 Introduction

In view of the rapid development on the advanced materials, the multilayered and function-

ally graded (FG) piezoelectric materials have widely been used as intelligent (or smart) structures for sensing and actuation purposes in recent years. Three-dimensional (3D) analysis for these types of structures is of much important for providing as a reference to develop an approximate two-dimensional (2D) theory and for assessing a variety of the relevant approximate theories and numerical methodologies. Determination of those 3D solutions of FG piezoelectric plates and shells therefore becomes an attractive research subject.

The state space approach is a conventional and efficient method for the 3D analysis of an elastic body. It has been successfully applied for the static, dynamic and buckling analyses of homogeneous elastic and laminated composite structures in the literature (Vlasov, 1957; Buefler, 1971; Fan and Ye, 1990; Soldatos and Hadjigeorgiou, 1990; Fan and Zhang, 1992). Introduction of the state space method and comprehensive literature review on its application to 3D problems of laminated composite plates and shells have been made by Ye (2003). Other analytical approaches for the previous 3D analyses of homogeneous elastic and laminated composite structures have also been proposed in the literature, such as the method of power series (Srinivas, 1970; Ren, 1989) and the method of perturbation (Rogers et al, 1992, 1995; Wu et al, 1996a, b; Wu and Chiu, 2002; Wu and Chi, 2005).

With the increase in usage of the intelligent (or smart) materials and structures, the 3D analysis of multilayered and FG piezoelectric plates and shells becomes as a new focus of researchers' attention. Based on the linear theory of piezoelectricity, several 3D static, dynamic and buckling analyses of piezoelectric laminates have been presented using the state space approach (Lee

¹ Corresponding author. Fax:+886-6-2370804, E-mail address: cpwu@mail.ncku.edu.tw.

² Department of Civil Engineering, National Cheng Kung University, Taiwan, ROC.

and Jiang, 1996; Chen et al, 2001; Kapuria and Achary, 2004; Han et al, 2006). The aforementioned 3D electro-elastic problems of piezoelectric laminates have also been studied by means of the Frobenius method (Heyliger and Brooks, 1996; Heyliger, 1997; Dumir et al, 1997) and the perturbation method (Wu et al, 2005; Wu and Lo, 2006; Wu and Syu, 2006; Wu et al, 2007). Several numerical methodologies, such as the reproducing kernel particle method, the meshless radial point interpolation method, the local Petrov-Galerkin method and the element-free Galerkin method, have been developed for the static and dynamic analyses of homogeneous piezoelectric and functionally graded piezoelectric structures (Wang et al, 2002; Dai et al, 2004, 2005; Sladek et al, 2006; Ferreira et al, 2005, 2006). Comprehensive reviews of theoretical analysis and numerical modeling for piezoelectric laminates have been presented by Saravanan and Heyliger (1999) and Gopinathan et al (2000).

The previous literature has reported some drawbacks of piezoelectric laminates such as huge inter-laminar stresses induced at interfaces between adjacent layers constituting the laminates, etc. This is mainly due to the material properties of the piezoelectric laminates having a sudden change at interfaces between adjacent layers. A new class of intelligent structures, namely FG piezoelectric plates and shells, has emerged until quite recently of which material properties are gradually varied through the thickness coordinate so that the aforementioned drawback of piezoelectric laminates can be eliminated. Hence, the 3D analysis of FG piezoelectric plates and shells becomes important for providing a better design of this type of intelligent structures.

Several 3D and accurate analyses of FG elastic and piezoelectric plates have been presented. A state space approach has been used for the 3D static analysis of FG piezoelectric plates by Zhong and Shang (2003). In their analysis, the material properties are assumed to obey the same exponent-law dependence on the thickness coordinate. It has been concluded that the proposed approach may be valid for arbitrary mechanical and electric lateral loads. Based on the pseudo-

Stroh formalism, Pan (2003) extended Pagano's solution process of laminated composite plates to the coupled analysis of FG elastic plates. In conjunction with the pseudo-Stroh formalism and the method of propagator matrix, Pan and Han (2005) have studied the exact analysis of FG and layered magneto-electro-elastic plates. Ramirez et al (2006) have presented the accurate solutions of FG elastic anisotropic plates using a discrete layer theory in combination with the Ritz method. It has been illustrated that any continuous functions representing the variation of material properties along the thickness coordinate may be incorporated in the discrete layer model.

After a close literature survey, we found that the literature dealing with the 3D analysis of FG piezoelectric shells is scarce in comparison with that of FG piezoelectric plates. The present paper therefore aims to extendedly apply the state space approach to the 3D analysis of doubly curved FG piezoelectric shells. The material properties are assumed to obey the identical exponent-law exponentially varied with the thickness coordinate. A set of dimensionless field variables is defined and introduced in the present formulation to prevent from the ill-conditioned problem in the relevant computation. The present formulation includes the formulation of FG piezoelectric plates as a special case by letting the curvature radius an infinitely large value. For the comparison purpose, the present formulation is further reduced and applied to the 3D analysis of laminated elastic and piezoelectric plates. The accuracy and convergence rate of present solutions are validated by making the comparison with the 3D solutions available in the literature. The through-the-thickness distributions of inter-laminar stresses are mainly concerned. It is illustrated that the phenomenon of inter-laminar stress concentration is eliminated in the FG piezoelectric shells. The influences of the radius-to-thickness ratio, the span-to-thickness ratio and the material property gradient index on the static behavior of FG piezoelectric shells under electro-mechanical loads are studied.

2 Basic equations of 3D piezoelectricity

Consider a doubly curved functionally graded piezoelectric shell as shown in Fig. 1 where the thickness of the shell is $2h$. A set of the orthogonal curvilinear coordinates α, β, ζ is adopted and located on the middle surface of the shell. R_α and R_β denote the curvature radii to the middle surface; a_α and a_β are the curvilinear dimensions in α and β directions, respectively.

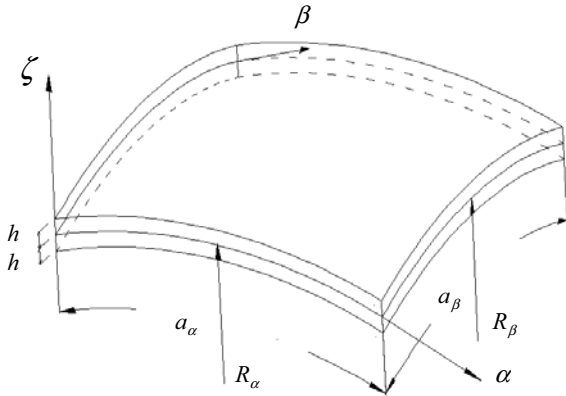


Figure 1: The geometry and coordinates of a doubly curved shell.

The linear constitutive equations valid for the nature of symmetry class of the piezoelectric material considered are given by

$$\begin{Bmatrix} \sigma_\alpha \\ \sigma_\beta \\ \sigma_\zeta \\ \tau_{\beta\zeta} \\ \tau_{\alpha\zeta} \\ \tau_{\alpha\beta} \end{Bmatrix} = \begin{bmatrix} c_{11} & c_{12} & c_{13} & 0 & 0 & 0 \\ c_{12} & c_{22} & c_{23} & 0 & 0 & 0 \\ c_{13} & c_{23} & c_{33} & 0 & 0 & 0 \\ 0 & 0 & 0 & c_{44} & 0 & 0 \\ 0 & 0 & 0 & 0 & c_{55} & 0 \\ 0 & 0 & 0 & 0 & 0 & c_{66} \end{bmatrix} \begin{Bmatrix} \varepsilon_\alpha \\ \varepsilon_\beta \\ \varepsilon_\zeta \\ \gamma_{\beta\zeta} \\ \gamma_{\alpha\zeta} \\ \gamma_{\alpha\beta} \end{Bmatrix} - \begin{bmatrix} 0 & 0 & e_{31} \\ 0 & 0 & e_{32} \\ 0 & 0 & e_{33} \\ 0 & e_{24} & 0 \\ e_{15} & 0 & 0 \\ 0 & 0 & 0 \end{bmatrix} \begin{Bmatrix} E_\alpha \\ E_\beta \\ E_\zeta \end{Bmatrix} \quad (1)$$

$$\begin{Bmatrix} D_\alpha \\ D_\beta \\ D_\zeta \end{Bmatrix} = \begin{bmatrix} 0 & 0 & 0 & 0 & e_{15} & 0 \\ 0 & 0 & 0 & e_{24} & 0 & 0 \\ e_{31} & e_{32} & e_{33} & 0 & 0 & 0 \end{bmatrix} \begin{Bmatrix} \varepsilon_\alpha \\ \varepsilon_\beta \\ \varepsilon_\zeta \\ \gamma_{\beta\zeta} \\ \gamma_{\alpha\zeta} \\ \gamma_{\alpha\beta} \end{Bmatrix} + \begin{bmatrix} \eta_{11} & 0 & 0 \\ 0 & \eta_{22} & 0 \\ 0 & 0 & \eta_{33} \end{bmatrix} \begin{Bmatrix} E_\alpha \\ E_\beta \\ E_\zeta \end{Bmatrix}, \quad (2)$$

where $(\sigma_\alpha, \sigma_\beta, \sigma_\zeta, \tau_{\alpha\zeta}, \tau_{\beta\zeta}, \tau_{\alpha\beta})$ and $(\varepsilon_\alpha, \varepsilon_\beta, \varepsilon_\zeta, \gamma_{\alpha\zeta}, \gamma_{\beta\zeta}, \gamma_{\alpha\beta})$ denote the stress and strain components, respectively. $(D_\alpha, D_\beta, D_\zeta)$ and $(E_\alpha, E_\beta, E_\zeta)$ denote the components of electric displacement and electric field, respectively. c_{ij}, e_{ij} and η_{ij} are the elastic coefficients, piezoelectric coefficients and dielectric coefficients, respectively, relative to the geometrical axes of the shell. The material is regarded to be heterogeneous through the thickness coordinate (i.e., $c_{ij}(\zeta), e_{ij}(\zeta)$ and $\eta_{ij}(\zeta)$).

The kinematic equations in terms of the curvilinear coordinates α, β and ζ are

$$\begin{aligned} \varepsilon_\alpha &= (1/\gamma_\alpha)(u_{\alpha,\alpha} + u_\zeta/R_\alpha), \\ \varepsilon_\beta &= (1/\gamma_\beta)(u_{\beta,\beta} + u_\zeta/R_\beta), \\ \varepsilon_\zeta &= u_{\zeta,\zeta}, \\ \gamma_{\beta\zeta} &= (1/\gamma_\beta)u_{\zeta,\beta} + u_{\beta,\zeta} - (u_\beta/\gamma_\beta R_\beta), \\ \gamma_{\alpha\zeta} &= (1/\gamma_\alpha)u_{\zeta,\alpha} + u_{\alpha,\zeta} - (u_\alpha/\gamma_\alpha R_\alpha), \\ \gamma_{\alpha\beta} &= (1/\gamma_\alpha)u_{\beta,\alpha} + (1/\gamma_\beta)u_{\alpha,\beta}, \end{aligned} \quad (3)$$

in which $\gamma_\alpha = 1 + (\zeta/R_\alpha)$; $\gamma_\beta = 1 + (\zeta/R_\beta)$; u_α, u_β and u_ζ are the displacement components.

The stress equilibrium equations without body forces are given by

$$\begin{aligned} \gamma_\beta \sigma_{\alpha,\alpha} + \gamma_\alpha \tau_{\alpha\beta,\beta} + \gamma_\alpha \gamma_\beta \tau_{\alpha\zeta,\zeta} \\ + [(2/R_\alpha) + (1/R_\beta) + (3\zeta/R_\alpha R_\beta)] \tau_{\alpha\zeta} = 0, \end{aligned} \quad (4)$$

$$\begin{aligned} \gamma_\alpha \sigma_{\beta,\beta} + \gamma_\beta \tau_{\alpha\beta,\alpha} + \gamma_\alpha \gamma_\beta \tau_{\beta\zeta,\zeta} \\ + [(1/R_\alpha) + (2/R_\beta) + (3\zeta/R_\alpha R_\beta)] \tau_{\beta\zeta} = 0, \end{aligned} \quad (5)$$

$$\begin{aligned} & \gamma_\beta \tau_{\alpha\zeta,\alpha} + \gamma_\alpha \tau_{\beta\zeta,\beta} + \gamma_\alpha \gamma_\beta \sigma_{\zeta,\zeta} \\ & + [(1/R_\alpha) + (1/R_\beta) + (2\zeta/R_\alpha R_\beta)] \sigma_\zeta \\ & - (\gamma_\beta/R_\alpha) \sigma_\alpha - (\gamma_\alpha/R_\beta) \sigma_\beta = 0. \end{aligned} \quad (6)$$

The charge equation of the piezoelectric material in curvilinear coordinates α , β and ζ is

$$\begin{aligned} & \gamma_\beta D_{\alpha,\alpha} + \gamma_\alpha D_{\beta,\beta} + \gamma_\alpha \gamma_\beta D_{\zeta,\zeta} \\ & + [(\gamma_\beta/R_\alpha) + (\gamma_\alpha/R_\beta)] D_\zeta = 0. \end{aligned} \quad (7)$$

The relations between the electric field and electric potential in curvilinear coordinates α , β and ζ are

$$\begin{aligned} E_\alpha &= -(1/\gamma_\alpha) \Phi_{,\alpha}, \\ E_\beta &= -(1/\gamma_\beta) \Phi_{,\beta}, \\ E_\zeta &= -\Phi_{,\zeta}, \end{aligned} \quad (8)$$

where Φ denotes the electric potential.

The boundary conditions of the problem are specified as follows:

On the lateral surfaces the transverse loads and either electric potential or normal electric displacement are prescribed,

$$[\tau_{\alpha\zeta} \quad \tau_{\beta\zeta}] = [0 \quad 0] \quad \text{on } \zeta = \pm h, \quad (9a)$$

$$\sigma_\zeta = \bar{q}_\zeta^\pm(\alpha, \beta) \quad \text{on } \zeta = \pm h, \quad (9b)$$

either

$$\Phi = \bar{\Phi}_\zeta^\pm(\alpha, \beta) \text{ or } \bar{D}_\zeta = \bar{D}_\zeta^\pm(\alpha, \beta) \text{ on } \zeta = \pm h. \quad (10)$$

The edge boundary conditions of fully simple supports require the following quantities be satisfied:

$$\sigma_\alpha = u_\beta = u_\zeta = 0, \text{ at } \alpha = 0 \text{ and } \alpha = a_\alpha; \quad (11a)$$

$$\sigma_\beta = u_\alpha = u_\zeta = 0, \text{ at } \beta = 0 \text{ and } \beta = a_\beta. \quad (11b)$$

In addition, the edges are suitably grounded so that the electric potential Φ at the edges are zero and given by

$$\Phi = 0. \quad (12)$$

3 Nondimensionalization and the state equations

To scale the numerical values of all the field variables in an appropriate range, we define a set of dimensionless coordinates and variables as follows.

$$\begin{aligned} x &= \alpha/\sqrt{Rh}, & y &= \beta/\sqrt{Rh}, & z &= \zeta/h; \\ u &= u_\alpha/\sqrt{Rh} & v &= u_\beta/\sqrt{Rh}, & w &= u_\zeta/R; \\ R_x &= R_\alpha/R, & R_y &= R_\beta/R; \\ \sigma_x &= \sigma_\alpha/Q, & \sigma_y &= \sigma_\beta/Q, & \sigma_z &= \sigma_\zeta R/Qh; \\ \tau_{xz} &= \tau_{\alpha\zeta}/Q\sqrt{h/R}, & \tau_{yz} &= \tau_{\beta\zeta}/Q\sqrt{h/R}, \\ \tau_{xy} &= \tau_{\alpha\beta}/Q; & D_x &= D_\alpha/e\sqrt{h/R}, \\ D_y &= D_\beta/e\sqrt{h/R}, & D_z &= D_\zeta/e; \\ \phi &= \Phi e/Qh; \end{aligned} \quad (13)$$

where R , Q and e denote a characteristic length of the shell, the reference elastic and piezoelectric moduli, respectively.

In the present formulation the elastic displacements (u_α , u_β , u_ζ), the transverse shear and normal stresses ($\tau_{\alpha\zeta}$, $\tau_{\beta\zeta}$, σ_ζ), the electric potential (Φ) and normal electric displacement (D_ζ) are selected as the primary field variables. The other field variables such as the in-surface stresses (σ_α , σ_β and $\tau_{\alpha\beta}$), electric displacements (D_α , D_β), the components of strain (ϵ_α , ϵ_β , ϵ_ζ , $\gamma_{\alpha\zeta}$, $\gamma_{\beta\zeta}$, $\gamma_{\alpha\beta}$) and electric field (E_α , E_β , E_ζ) are the secondary field variables and can be determined from the primary field variables. In order to make the complicated system of basic 3D equations suitable for mathematical treatment, we directly eliminate the secondary field variables from Eqs. (1)-(12) and then substitute the dimensionless field variables (Eq. (13)) in the resulting equations. That leads to a system of state equations with variable coefficients as follows:

$$\frac{\partial}{\partial z} \begin{bmatrix} u \\ v \\ \sigma_z \\ D_z \\ \tau_{xz} \\ \tau_{yz} \\ w \\ \phi \end{bmatrix} = \begin{bmatrix} d_{11} & 0 & 0 & 0 & d_{15} & 0 & d_{17} & d_{18} \\ 0 & d_{22} & 0 & 0 & 0 & d_{26} & d_{27} & d_{28} \\ d_{31} & d_{32} & d_{33} & d_{34} & d_{17} & d_{27} & d_{37} & 0 \\ 0 & 0 & 0 & d_{44} & d_{18} & d_{28} & 0 & d_{48} \\ d_{51} & d_{52} & d_{53} & d_{54} & d_{55} & 0 & d_{57} & 0 \\ d_{61} & d_{62} & d_{63} & d_{64} & 0 & d_{66} & d_{67} & 0 \\ d_{53} & d_{63} & d_{73} & d_{74} & 0 & 0 & d_{77} & 0 \\ d_{54} & d_{64} & d_{74} & d_{84} & 0 & 0 & d_{87} & 0 \end{bmatrix} \begin{bmatrix} u \\ v \\ \sigma_z \\ D_z \\ \tau_{xz} \\ \tau_{yz} \\ w \\ \phi \end{bmatrix} \quad (14)$$

where d_{ij} are the relevant differential operators containing the derivatives with respect to the x and y coordinates only, not z coordinate, and given in Appendix A.

It is noted that the previous system of state equations for piezoelectric shells (Eq. (14)) can be further reduced as those for piezoelectric plates by letting $1/R_x = 0$ and $1/R_y = 0$. They are given as

$$\frac{\partial}{\partial z} \begin{bmatrix} u \\ v \\ \sigma_z \\ D_z \\ \tau_{xz} \\ \tau_{yz} \\ w \\ \phi \end{bmatrix} = \begin{bmatrix} 0 & 0 & 0 & 0 & l_{15} & 0 & l_{17} & l_{18} \\ 0 & 0 & 0 & 0 & 0 & l_{26} & l_{27} & l_{28} \\ 0 & 0 & 0 & 0 & l_{17} & l_{27} & 0 & 0 \\ 0 & 0 & 0 & 0 & l_{18} & l_{28} & 0 & l_{48} \\ l_{51} & l_{52} & l_{53} & l_{54} & 0 & 0 & 0 & 0 \\ l_{61} & l_{62} & l_{63} & l_{64} & 0 & 0 & 0 & 0 \\ l_{53} & l_{63} & l_{73} & l_{74} & 0 & 0 & 0 & 0 \\ l_{54} & l_{64} & l_{74} & l_{84} & 0 & 0 & 0 & 0 \end{bmatrix} \begin{bmatrix} u \\ v \\ \sigma_z \\ D_z \\ \tau_{xz} \\ \tau_{yz} \\ w \\ \phi \end{bmatrix} \quad (15)$$

where the relevant differential operators l_{ij} are given in Appendix B.

According to Eq. (15), we include the state space analysis of FG piezoelectric plates as a special case of the present formulation.

The in-surface stresses and electric displacements are dependent field variables that can be expressed in terms of the primary variables in the following form

$$\boldsymbol{\sigma}_p = \mathbf{B}_1 \mathbf{u} + \mathbf{B}_1 w + \mathbf{B}_3 \sigma_z + \mathbf{B}_4 D_z \quad (16)$$

$$\mathbf{d} = \mathbf{B}_5 \boldsymbol{\sigma}_s + \mathbf{B}_6 \phi, \quad (17)$$

where

$$\boldsymbol{\sigma}_p = \begin{Bmatrix} \sigma_x \\ \sigma_y \\ \tau_{xy} \end{Bmatrix},$$

$$\mathbf{B}_1 = \begin{bmatrix} \tilde{b}_{11} & \tilde{b}_{12} \\ \tilde{b}_{21} & \tilde{b}_{22} \\ \tilde{b}_{31} & \tilde{b}_{32} \end{bmatrix}, \quad \mathbf{B}_2 = \begin{bmatrix} \tilde{b}_{13} \\ \tilde{b}_{23} \\ \tilde{b}_{33} \end{bmatrix},$$

$$\mathbf{B}_3 = \begin{bmatrix} \tilde{b}_{14} \\ \tilde{b}_{24} \\ \tilde{b}_{34} \end{bmatrix}, \quad \mathbf{B}_4 = \begin{bmatrix} \tilde{b}_{15} \\ \tilde{b}_{25} \\ \tilde{b}_{35} \end{bmatrix},$$

$$\mathbf{B}_5 = \begin{bmatrix} \tilde{b}_{41} & \tilde{b}_{42} \\ \tilde{b}_{51} & \tilde{b}_{52} \end{bmatrix}, \quad \mathbf{B}_6 = \begin{bmatrix} \tilde{b}_{43} \\ \tilde{b}_{53} \end{bmatrix},$$

and \tilde{b}_{ij} are given in Appendix C.

The dimensionless form of boundary conditions of the problem are specified as follows:

On the lateral surface the transverse load and electric potential are prescribed,

$$[\tau_{xz} \quad \tau_y] = [0 \quad 0] \quad \text{on } z = \pm 1, \quad (18a)$$

$$\sigma_z = \bar{q}_z^\pm(x, y) \quad \text{on } z = \pm 1, \quad (18b)$$

either

$$\phi = \bar{\phi}_z^\pm(x, y) \text{ or } D_z = \bar{D}_z^\pm(x, y) \quad \text{on } z = \pm 1, \quad (19)$$

where $\bar{q}_z^\pm = \bar{q}_z^\pm R/Qh$; $\bar{\phi}_z^\pm = \bar{\Phi}_z^\pm e/hQ$; $\bar{D}_z^\pm = \bar{D}_z^\pm/e$.

At the edges the following quantities is satisfied:

$$\sigma_x = v = w = 0 \text{ at } x = 0 \text{ and } x = a_\alpha/\sqrt{Rh}, \quad (20a)$$

$$\sigma_y = u = w = 0 \text{ at } y = 0 \text{ and } y = a_\beta/\sqrt{Rh}. \quad (20b)$$

In addition,

$$\phi = 0. \quad (21)$$

4 Applications to the benchmark problems

4.1 Double Fourier series expansion

The edge boundary conditions of the shells are considered as fully simple supports in the analysis. By means of the method of separation of variables, the primary field variables are expanded as the following forms of double Fourier series so that the boundary conditions of simply supported edges are exactly satisfied.

$$u = \sum_{m=1}^{\infty} \sum_{n=1}^{\infty} u_{mn}(z) \cos \tilde{m}x \sin \tilde{n}y, \tag{22}$$

$$v = \sum_{m=1}^{\infty} \sum_{n=1}^{\infty} v_{mn}(z) \sin \tilde{m}x \cos \tilde{n}y, \tag{23}$$

$$w = \sum_{m=1}^{\infty} \sum_{n=1}^{\infty} w_{mn}(z) \sin \tilde{m}x \sin \tilde{n}y, \tag{24}$$

$$\tau_{xz} = \sum_{m=1}^{\infty} \sum_{n=1}^{\infty} \tau_{xzm}(z) \cos \tilde{m}x \sin \tilde{n}y, \tag{25}$$

$$\tau_{yz} = \sum_{m=1}^{\infty} \sum_{n=1}^{\infty} \tau_{yzm}(z) \sin \tilde{m}x \cos \tilde{n}y, \tag{26}$$

$$\sigma_z = \sum_{m=1}^{\infty} \sum_{n=1}^{\infty} \sigma_{zmn}(z) \sin \tilde{m}x \sin \tilde{n}y, \tag{27}$$

$$D_z = \sum_{m=1}^{\infty} \sum_{n=1}^{\infty} D_{zmn}(z) \sin \tilde{m}x \sin \tilde{n}y, \tag{28}$$

$$\phi = \sum_{m=1}^{\infty} \sum_{n=1}^{\infty} \phi_{mn}(z) \sin \tilde{m}x \sin \tilde{n}y, \tag{29}$$

where $\tilde{m} = m\pi\sqrt{Rh}/a_\alpha$ and $\tilde{n} = n\pi\sqrt{Rh}/a_\beta$.

Substituting Eqs. (22)-(29) in Eq. (14) yields

$$\frac{\partial}{\partial z} \mathbf{F}(z) = \mathbf{D}(z)\mathbf{F}(z), \tag{30}$$

where $\mathbf{F}(z)$ is called the state vector of the shell and given as $\mathbf{F}^T(z) = [u_{mn} \ v_{mn} \ \sigma_{zmn} \ D_{zmn} \ \tau_{xzm} \ \tau_{yzm} \ w_{mn} \ \phi_{mn}]$; the components of $\mathbf{F}(z)$ are state variables; $\mathbf{D}(z)$ is called the coefficient matrix (or the system matrix) and given as

$$\mathbf{D}(z) =$$

$$\begin{bmatrix} \bar{d}_{11} & 0 & 0 & 0 & \bar{d}_{15} & 0 & \bar{d}_{17} & \bar{d}_{18} \\ 0 & \bar{d}_{22} & 0 & 0 & 0 & \bar{d}_{26} & \bar{d}_{27} & \bar{d}_{28} \\ \bar{d}_{31} & \bar{d}_{32} & \bar{d}_{33} & \bar{d}_{34} & -\bar{d}_{17} & -\bar{d}_{27} & \bar{d}_{37} & 0 \\ 0 & 0 & 0 & \bar{d}_{44} & -\bar{d}_{18} & -\bar{d}_{28} & 0 & \bar{d}_{48} \\ \bar{d}_{51} & \bar{d}_{52} & \bar{d}_{53} & \bar{d}_{54} & \bar{d}_{55} & 0 & \bar{d}_{57} & 0 \\ \bar{d}_{61} & \bar{d}_{62} & \bar{d}_{63} & \bar{d}_{64} & 0 & \bar{d}_{66} & \bar{d}_{67} & 0 \\ -\bar{d}_{53} & -\bar{d}_{63} & \bar{d}_{73} & \bar{d}_{74} & 0 & 0 & \bar{d}_{77} & 0 \\ -\bar{d}_{54} & -\bar{d}_{64} & \bar{d}_{74} & \bar{d}_{84} & 0 & 0 & -\bar{d}_{34} & 0 \end{bmatrix},$$

and \bar{d}_{ij} are functions of z .

Practically, the system of Eq. (30) can be compared to a linear time-varying system in structural dynamics problems where the prescribed conditions of electric and elastic field variables at the bottom surface of the shell are regarded as the initial state of the system. It is well known that a linear time-varying system is much more difficult to be solved than a time-invariant system of the same order. A successive approximation method (Ye, 2003) is used to solve Eq. (30) by solving a series of state equations of a time-invariant system.

4.2 The method of propagator matrix

Based on the successive approximation method, we artificially divide the thickness of the shell into NL layers with a uniform and small thickness. The dimensionless thickness coordinates of the top and bottom surfaces of a typical k^{th} -layer are defined as z_k and z_{k-1} , and the thickness of the k^{th} -layer is $h_k = (z_k - z_{k-1})h = 2h/NL$. For the typical k^{th} -layer, Eq. (30) can be approximately represented as

$$\frac{\partial}{\partial z} \mathbf{F}(z) = \bar{\mathbf{D}}_k \mathbf{F}(z) \quad z_{k-1} \leq z \leq z_k, \tag{31}$$

where $\bar{\mathbf{D}}_k$ is a 8×8 constant coefficient matrix and $\bar{\mathbf{D}}_k = \mathbf{D}(\frac{z_k+z_{k-1}}{2})$.

With a known state vector at the bottom surface of the k^{th} -layer (\mathbf{F}_{k-1}), the solution of equation (31) is

$$\begin{aligned} \mathbf{F}(z) &= e^{\bar{\mathbf{D}}_k(z-z_{k-1})} \mathbf{F}_{k-1} \\ &= \mathbf{M}_k e^{\Lambda_k(z-z_{k-1})} \mathbf{M}_k^{-1} \mathbf{F}_{k-1}, \end{aligned} \tag{32}$$

where \mathbf{M}_k is the modal matrix of $\bar{\mathbf{D}}_k$ consisting of eight independent eigenvectors; $\mathbf{F}_{k-1} = \mathbf{F}(z_{k-1})$;

$e^{\Lambda_k z}$ is a 8×8 diagonal matrix and given by

$$e^{\Lambda_k z} = \begin{bmatrix} e^{\lambda_1 z} & 0 & \dots & 0 \\ 0 & e^{\lambda_2 z} & \dots & 0 \\ \vdots & \vdots & \ddots & \vdots \\ 0 & 0 & \dots & e^{\lambda_8 z} \end{bmatrix}$$

in which $\lambda_1, \lambda_2, \dots, \lambda_8$ are the set of eigen values of $\bar{\mathbf{D}}_k$.

According to Eq. (32), the state vector within the k^{th} -layer can be determined. By using $z = z_k$, the state vector of the top surface of the k^{th} -layer is then determined as follows.

$$\mathbf{F}_k = \mathbf{R}_k \mathbf{F}_{k-1}, \quad (33)$$

where $\mathbf{F}_k = \mathbf{F}(z_k)$; $\mathbf{R}_k = \mathbf{M}_k e^{\Lambda_k h_k} \mathbf{M}_k^{-1}$.

By analogy, the state vectors between the top and bottom surfaces of the shell are linked by

$$\begin{aligned} \mathbf{F}_{NL} &= \mathbf{R}_{NL} \mathbf{F}_{(NL-1)} \\ &= \mathbf{R}_{NL} \mathbf{R}_{(NL-1)} \cdots \mathbf{R}_1 \mathbf{F}_0. \end{aligned} \quad (34)$$

By defining a symbol of consecutive multiplication, we rewrite Eq. (34) in the form of

$$\mathbf{F}_{NL} = \left(\prod_{k=1}^{NL} \mathbf{R}_k \right) \mathbf{F}_0, \quad (35)$$

where $\prod_{k=1}^{NL} \mathbf{R}_k = \mathbf{R}_{NL} \mathbf{R}_{(NL-1)} \cdots \mathbf{R}_2 \mathbf{R}_1$.

Equation (35) represents a set of simultaneous algebraic equations. After imposing the boundary conditions prescribed on the lateral surfaces, Eqs. (18) and (19), the other unknowns in state vectors of lateral surfaces of the shell can then be determined. After then, the state vector through the thickness coordinate of the shell can be obtained by

$$\begin{aligned} \mathbf{F}(z) &= \mathbf{M}_k e^{\Lambda_k (z-z_{k-1})} \mathbf{M}_k^{-1} \mathbf{F}_{k-1} \\ &= \mathbf{M}_k e^{\Lambda_k (z-z_{k-1})} \mathbf{M}_k^{-1} \left(\prod_{i=1}^{k-1} \mathbf{R}_i \right) \mathbf{F}_0. \end{aligned} \quad (36)$$

Equations (35)-(36) provide approximate solutions of a system of the state equations with variable coefficients. The accurate solutions of the system can be approached by increasing the total number of artificially divided layers.

5 Illustrative examples

The 3D static analysis of simply supported, doubly curved functionally graded piezoelectric shells under electro-mechanical loads is studied using the aforementioned formulation. In illustrative examples, we consider five cases of electro-mechanical loads as follows:

Case 1.

$$\begin{aligned} \bar{q}_\zeta^+ &= q_0 \sin(\pi\alpha/a_\alpha) \sin(\pi\beta/a_\beta) \text{ N/m}^2, \\ \bar{q}_\zeta^- &= 0 \text{ N/m}^2. \end{aligned} \quad (37)$$

Case 2.

$$\begin{aligned} \bar{q}_\zeta^+ &= q_0 \sin(\pi\beta/a_\beta) \text{ N/m}^2, \\ \bar{q}_\zeta^- &= 0 \text{ N/m}^2; \\ \bar{\Phi}_\zeta^+ &= 0 \text{ C/m}^2, \\ \bar{\Phi}_\zeta^- &= 0 \text{ C/m}^2. \end{aligned} \quad (38)$$

Case 3.

$$\begin{aligned} \bar{q}_\zeta^+ &= 0 \text{ N/m}^2, \\ \bar{q}_\zeta^- &= 0 \text{ N/m}^2; \\ \bar{\Phi}_\zeta^+ &= \Phi_0 \sin(\pi\beta/a_\beta) \text{ C/m}^2, \\ \bar{\Phi}_\zeta^- &= 0 \text{ C/m}^2. \end{aligned} \quad (39)$$

Case 4.

$$\begin{aligned} \bar{q}_\zeta^+ &= q_0 \sin(\pi\beta/a_\beta) \text{ N/m}^2, \\ \bar{q}_\zeta^- &= 0 \text{ N/m}^2; \\ \bar{D}_\zeta^+ &= 0 \text{ C/m}^2, \\ \bar{D}_\zeta^- &= 0 \text{ C/m}^2. \end{aligned} \quad (40)$$

Case 5.

$$\begin{aligned} \bar{q}_\zeta^+ &= 0 \text{ N/m}^2, \\ \bar{q}_\zeta^- &= 0 \text{ N/m}^2; \\ \bar{D}_\zeta^+ &= D_0 \sin(\pi\beta/a_\beta) \text{ C/m}^2, \\ \bar{D}_\zeta^- &= 0 \text{ C/m}^2. \end{aligned} \quad (41)$$

The structural behavior of three types of piezoelectric shells are evaluated and the through-the-thickness distributions of material properties are described as follows:

Type 1 single-layer piezoelectric shells

For a Type 1 shell, the material properties are assumed as homogeneous, independent upon the thickness coordinate, and are given by

$$m_{ij}(\zeta) = m_{ij}, \quad (42)$$

where m_{ij} represent the coefficients of c_{ij} , e_{ij} and η_{ij} and are constants.

Type 2 multilayered piezoelectric shells

For a Type 2 shell, the material properties are assumed as the layerwise step functions through the thickness and are given by

$$m_{ij}(\zeta) = \sum_{k=1}^{NL} m_{ij}^{(k)} [H(\zeta - \zeta_{k-1}) - H(\zeta - \zeta_k)], \quad (43)$$

where $H(\zeta)$ is the Heaviside function; ζ_{k-1} and ζ_k are the thickness coordinates measured from the middle surface of the shell to the bottom and top surfaces of the k^{th} -layer, respectively.

Type 3 exponent-law class of functionally graded piezoelectric shells

For a Type 3 shell, the material properties are assumed to obey the identical exponent-law varied exponentially with the thickness coordinate and are given by

$$m_{ij} = m_{ij}^{(b)} e^{\alpha[(\zeta+h)/2h]}, \quad (44)$$

where $m_{ij}^{(b)}$ are the material properties of bottom surface; α is the material property gradient index which represents the degree of the material gradient along the thickness coordinate and is taken as the values of -3.0, -1.5, 0, 1.5, 3, respectively, in the present analysis.

As we aforementioned, the FG shell is considered to be divided into NL individual homogeneous layers in the present state space formulation. Hence, for a typical k^{th} -layer the material properties $m_{ij}^{(k)}$ are determined in a thickness average sense and are given as

$$m_{ij}^{(k)} = \frac{1}{h_k} \int_{\zeta_{k-1}}^{\zeta_k} m_{ij}(\zeta) d\zeta$$

$$= \left(\frac{2h}{h_k \alpha} \right) e^{0.5\alpha} m_{ij}^{(b)} \left[e^{(\alpha/2h)\zeta_k} - e^{(\alpha/2h)\zeta_{k-1}} \right] \quad (\alpha \neq 0), \quad (45a)$$

$$m_{ij}^{(k)} = m_{ij}^{(b)} \quad (\alpha = 0). \quad (45b)$$

It is noted that the formulations for static behavior of single-layer homogeneous piezoelectric shells and FG elastic shells are also regarded as the special cases of the present formulation by letting $\alpha = 0$ and $e_{ij} = 0$, respectively.

5.1 Multilayered Elastic Shells

For the comparison purpose, the present state space formulation is applied for the analysis of a simply-supported, $[0^\circ/90^\circ]$ laminated doubly curved shell under the loading condition of Case 1 in Table 2 where 0° -layer is the upper layer and 90° -layer is the lower layer. The orthotropic material considered is elastic and orthotropic and its properties are: $E_L/E_T = 25$, $G_{LT}/E_T = 0.5$, $G_{TT}/E_T = 0.2$, $\nu_{LT} = \nu_{TT} = 0.25$, $E_T = 6.89 \times 10^9 \text{N/m}^2$. The geometric parameters are taken as $R_\alpha/a_\alpha = 5$, $R_\beta/a_\beta = 10$, $a_\alpha/a_\beta = 1$ and $S = a_\alpha/2h = 10$. The dimensionless field variables are defined as $\bar{\sigma}_{ij} = \sigma_{ij}/q_0$ and $\bar{w} = u_\zeta(2h)^3 E_T (10^3)/q_0 (a_\alpha)^4$. The accuracy and the convergence rate of the present solutions are evaluated in comparison with the 3D asymptotic solution available in the literature (Wu et al, 1996a). It is shown that the convergence rate of the present solution is rapid and the convergent solution is in excellent agreement with the 3D asymptotic solution.

5.2 Single-layer Piezoelectric Shells

The present state space formulation is also used for the coupled analysis of simply-supported, homogeneous piezoelectric cylindrical shells under the cylindrical bending type of applied mechanical load and applied electric potential (Case 2 and Case 3) in Tables 3-4, respectively. The shells are considered to be composed of polyvinylidene fluoride (PVDF) polarized along the radial direction. The elastic, piezoelectric and dielectric properties of PVDF material are given in Table 1. The dimensionless variables are denoted as the

Table 1: Elastic, piezoelectric and dielectric properties of composite and piezoelectric materials

Moduli	PVDF	PZT-4	Orthotropic material
c_{11} (GPa)	3.0	138.499	7.3802
c_{22}	3.0	138.499	173.406
c_{33}	3.0	114.745	7.3802
c_{12}	1.5	77.371	2.3121
c_{13}	1.5	73.643	1.8682
c_{23}	1.5	73.643	2.3121
c_{44}	0.75	25.6	3.445
c_{55}	0.75	25.6	1.378
c_{66}	0.75	30.6	3.445
e_{24} (C/m ²)	0.0	12.72	0
e_{15}	0.0	12.72	0
e_{31}	-0.15e-02	-5.2	0
e_{32}	0.285e-01	-5.2	0
e_{33}	-0.51e-01	15.08	0
η_{11} (F/m)	0.1062e-09	1.306e-08	1.53e-08
η_{22}	0.1062e-09	1.306e-08	1.53e-08
η_{33}	0.1062e-09	1.151e-08	1.53e-08

same forms of those in the Reference (Dumir et al, 1997) and given as follows:

For the cases of applied mechanical load (Case 2),

$$\begin{aligned}
 (\bar{u}_\theta, \bar{u}_r) &= \frac{100Y_r}{2hS_R^4|q_0|} (u_\beta, u_\zeta), \\
 (\bar{\sigma}_x, \bar{\sigma}_\theta, \bar{\sigma}_r, \bar{\tau}_{\theta r}) &= (\sigma_\alpha/S_R^2, \sigma_\beta/S_R^2, \sigma_\zeta, \tau_{\beta\zeta}/S_R) / |q_0|, \\
 (\bar{D}_\theta, \bar{D}_r) &= (D_\beta, D_\zeta) / |d_1| S_R |q_0|, \\
 \bar{\phi} &= |d_1| Y_r \phi / 2hS_R^2 |q_0|,
 \end{aligned} \tag{46}$$

and $S_R^2 = R_\beta/2h$, $Y_r = 2.0\text{GPa}$, $d_1 = -30 \times 10^{-12}\text{CN}^{-1}$;

For the cases of applied electric potential (Case 3),

$$\begin{aligned}
 (\bar{u}_\theta, \bar{u}_r) &= \frac{100}{|d_1| S_R |\phi_0|} (u_\beta, u_\zeta), \\
 (\bar{\sigma}_x, \bar{\sigma}_\theta, \bar{\sigma}_r, \bar{\tau}_{\theta r}) &= (\sigma_\alpha, S_R^2 \sigma_\beta, S_R^3 \sigma_\zeta, S_R^3 \tau_{\beta\zeta}) 2h/Y_r |d_1| |\phi_0|, \\
 (\bar{D}_\theta, \bar{D}_r) &= (S_R D_\beta, D_\zeta) 2h/|d_1|^2 Y_r |\phi_0|, \\
 \bar{\phi} &= \phi / |\phi_0|.
 \end{aligned} \tag{47}$$

Tables 3-4 show the present NL -layers solutions of elastic and electric field variables at crucial positions in the cylindrical shells. The geometric

parameters are taken as $R_\beta/2h = 4, 10, 100$ and $a_\beta/R_\beta = \pi/3$. It is shown that the convergence rate of elastic variables is more rapid than that of electric variables in the cases of applied mechanical load (Case 2). On the contrary, the convergence rate of elastic variables is slower than that of electric variables in the cases of applied electric potential (Case 3). The present 100-layers solutions are illustrated to be in excellent agreement with the 3D piezoelectricity solutions of both Dumir et al (1997) using the power series method and Wu and Syu (2007) using the method of perturbation.

5.3 FG Elastic Shells

The static behavior of doubly curved functionally graded elastic shells under the loading condition of Case 1 is considered in Figs. 2 and 3. The material properties of the shells are considered as orthotropic and obey the identical exponent-law exponentially varied through the thickness coordinate. The material properties of bottom surface are considered as orthotropic and are given in Table 1. The dimensionless field variables are defined as $(\bar{u}, \bar{w}) = (u_\alpha, u_\beta)(c^*/2hq_0)$, $(\bar{\sigma}_i, \bar{\tau}_{ij}) = (\sigma_i, \tau_{ij})/q_0$ and $c^* = 10^{10}\text{N/m}^2$.

Table 2: Mechanical field variables at crucial positions in a [0/90] laminated doubly curved shell under mechanical load (Case 1)

Z	Theories	$\bar{\sigma}_\alpha \left(\frac{u_\alpha}{z}, \frac{u_\beta}{z}, z \right) / q_0$	$\bar{\sigma}_\beta \left(\frac{u_\alpha}{z}, \frac{u_\beta}{z}, z \right) / q_0$	$\bar{\sigma}_\zeta \left(\frac{u_\alpha}{z}, \frac{u_\beta}{z}, z \right) / q_0$	$\bar{\tau}_{\alpha\zeta} \left(0, \frac{u_\beta}{z}, z \right) / q_0$	$\bar{\tau}_{\beta\zeta} \left(\frac{u_\alpha}{z}, 0, z \right) / q_0$	$\bar{w} \left(\frac{u_\alpha}{z}, \frac{u_\beta}{z}, z \right)$
1.0	Present solution $NL = 4$	72.2915	8.5832	1.0000	0.0000	0.0000	11.9177
	6	72.3661	8.5877	1.0000	0.0000	0.0000	11.9178
	8	72.4012	8.5898	1.0000	0.0000	0.0000	11.9178
	10	72.4215	8.5910	1.0000	0.0000	0.0000	11.9179
	20	72.4603	8.5935	1.0000	0.0000	0.0000	11.9179
	3D asymptotic solution (Wu et al., 1996)	72.5015	8.8503	1.0000	0.0000	0.0000	11.9190
0.0^\pm	Present solution $NL = 4$	-55.6223	1.9666	0.4296	1.3964	0.9963	11.9569
	6	(-1.5142)	(62.6979)	(0.4296)	(1.3964)	(0.9963)	(11.9569)
	8	-55.6562	1.9676	0.4296	1.3964	0.9963	11.9569
	10	(-1.5152)	(62.7315)	(0.4296)	(1.3964)	(0.9963)	(11.9569)
	20	-55.6749	1.9680	0.4296	1.3964	0.9963	11.9570
	3D asymptotic solution (Wu et al., 1996)	(-1.5158)	(62.7472)	(0.4296)	(1.3964)	(0.9963)	(11.9570)
-1.0	Present solution $NL = 4$	-55.6868	1.9683	0.4296	1.3964	0.9963	11.9570
	6	(-1.5162)	(62.7563)	(0.4296)	(1.3964)	(0.9963)	(11.9570)
	8	-55.7119	1.9687	0.4296	1.3964	0.9963	11.9570
	10	(-1.5171)	(62.7736)	(0.4296)	(1.3964)	(0.9963)	(11.9570)
	20	-55.7425	2.0775	0.4296	1.3965	0.9964	11.9581
	3D asymptotic solution (Wu et al., 1996)	(-1.5182)	(62.9176)	(0.4296)	(1.3965)	(0.9964)	(11.9581)
-1.0	Present solution $NL = 4$	-8.1885	-68.9423	0.0000	0.0000	0.0000	11.8897
	6	-8.1944	-68.9639	0.0000	0.0000	0.0000	11.8898
	8	-8.1974	-68.9758	0.0000	0.0000	0.0000	11.8898
	10	-8.1993	-68.9834	0.0000	0.0000	0.0000	11.8898
	20	-8.2031	-68.9994	0.0000	0.0000	0.0000	11.8899
	3D asymptotic solution (Wu et al., 1996)	-8.2074	-69.0028	0.0000	0.0000	0.0000	11.8910

Table 3: Mechanical and electric components at the crucial positions in single-layer piezoelectric cylindrical shells (PVDF) under cylindrical bending (Case 2)

R_β/h	Theories	$\bar{u}_\theta(0, +h)$	$\bar{u}_r\left(\frac{\theta_\alpha}{2}, 0\right)$	$\bar{\sigma}_x\left(\frac{\theta_\alpha}{2}, +h\right)$	$\bar{\sigma}_\theta\left(\frac{\theta_\alpha}{2}, +h\right)$	$\bar{\sigma}_r\left(\frac{\theta_\alpha}{2}, 0\right)$	$\bar{\tau}_{\theta r}(0, 0)$	$10^3\bar{\phi}\left(\frac{\theta_\alpha}{2}, 0\right)$	$10\bar{D}_r\left(\frac{\theta_\alpha}{2}, +h\right)$
4	Present solution $NL=4$	-0.9024	-21.1546	-0.2682	-0.7085	0.2202	-0.6245	2.4486	0.0746
		-0.8904	-21.1264	-0.2705	-0.7153	0.2185	-0.6241	2.4454	0.0450
		-0.8861	-21.1163	-0.2716	-0.7186	0.2178	-0.6240	2.4443	0.0346
		-0.8841	-21.1115	-0.2723	-0.7206	0.2175	-0.6239	2.4437	0.0298
		-0.8815	-21.1051	-0.2736	-0.7247	0.2171	-0.6238	2.4430	0.0234
		-0.8806	-21.1031	-0.2747	-0.7279	0.2170	-0.6238	2.4428	0.0214
10	3D solution Dumir et al. (1997) Wu and Syu (2007)	-0.8806	-21.10	-0.275	-0.7597	0.217	-0.6238	2.443	0.0213
		-0.8806	-21.1029	-0.2750	-0.7597	0.2170	-0.6238	2.4428	0.0213
		-3.5765	-17.6917	-0.2516	-0.7371	1.4207	-0.5894	2.5609	-0.0962
		-3.5741	-17.6877	-0.2527	-0.7403	1.4201	-0.5893	2.5604	-0.1302
		-3.5733	17.6863	-0.2532	-0.7419	1.4198	-0.5893	2.5602	-0.1421
		-3.5730	-17.6856	-0.2536	-0.7428	1.4197	-0.5893	2.5602	-0.1477
100	3D solution Dumir et al. (1997) Wu and Syu (2007)	-3.5724	-17.6847	-0.2542	-0.7446	1.4196	-0.5893	2.5600	-0.1550
		-3.5723	-17.6845	-0.2546	-0.7460	1.4195	-0.5893	2.5600	-0.1574
		-3.572	-17.68	-0.2548	-0.7514	1.420	-0.5893	2.560	-0.1575
		-3.5723	-17.6844	-0.2548	-0.7514	1.4195	-0.5893	2.5600	-0.1575
		-5.2969	-16.5535	-0.2507	-0.7490	18.3390	-0.5653	2.5035	-0.1416
		-5.2969	-16.5535	-0.2508	-0.7493	18.3390	-0.5653	2.5035	-0.1763
100	3D solution Dumir et al. (1997) Wu and Syu (2007)	-5.2969	-16.5535	-0.2509	-0.7495	18.3390	-0.5653	2.5035	-0.1885
		-5.2969	-16.5535	-0.2509	-0.7496	18.3389	-0.5653	2.5035	-0.1941
		-5.2969	-16.5535	-0.2510	-0.7500	18.3389	-0.5653	2.5035	-0.2016
		-5.2969	-16.5535	-0.2510	-0.7499	18.3389	-0.5653	2.5035	-0.2040
		-5.297	-16.55	-0.2510	-0.7500	18.34	-0.5653	2.504	-0.2041
		-5.2969	-16.5535	-0.2510	-0.7500	18.3389	-0.5653	2.5035	-0.2041

Table 4: Mechanical and electric components at the crucial positions in single-layer piezoelectric cylindrical shells (PVDF) under cylindrical bending (Case 3)

$R_\beta / (2h)$	Theories	$\bar{u}_\theta(0, +h)$	$\bar{u}_r\left(\frac{\theta_x}{2}, 0\right)$	$\bar{\sigma}_x\left(\frac{\theta_x}{2}, +h\right)$	$\bar{\sigma}_x\left(\frac{\theta_x}{2}, -h\right)$	$\bar{\sigma}_\theta\left(\frac{\theta_x}{2}, -h\right)$	$\bar{\tau}_{\theta r}\left(0, -\frac{h}{2}\right)$	$\bar{\phi}\left(\frac{\theta_x}{2}, 0\right)$	$\bar{D}_r\left(\frac{\theta_x}{2}, +h\right)$	
4	Present solution NL = 4	6	-28.7331	11.3436	-0.1408	-0.1431	-1.8802	0.3187	-0.4978	62.8186
		8	-28.7387	11.6501	-0.1370	-0.1413	-1.7962	0.3598	-0.4978	62.7903
		10	-28.7408	11.7573	-0.1353	-0.1402	-1.7429	0.3740	-0.4978	62.7805
		20	-28.7418	11.8070	-0.1343	-0.1395	-1.7072	0.3807	-0.4978	62.7760
		100	-28.7431	11.8732	-0.1324	-0.1378	-1.6273	0.3895	-0.4978	62.7699
	3D solution	Dumir et al. (1997)	-28.7436	11.8943	-0.1311	-0.1363	-1.5552	0.3924	-0.4978	62.7680
		3D solution								
		Dumir et al. (1997)	-28.74	11.90	-0.1307	-0.1359	-1.536	0.3925	-0.4978	62.77
		3D solution								
		Wu and Syu (2007)	-28.7436	11.8952	-0.1307	-0.1359	-1.5361	0.3925	-0.4978	62.7679
10	Present solution NL = 4	6	-26.6083	5.7244	-0.1068	-0.1116	-2.3780	0.2296	-0.5070	58.9664
		8	-26.5405	6.0662	-0.1052	-0.1108	-2.1450	0.3231	-0.5070	58.9653
		10	-26.5168	6.1858	-0.1044	-0.1103	-2.0026	0.3562	-0.5070	58.9649
		20	-26.5058	6.2412	-0.1040	-0.1100	-1.9088	0.3714	-0.5070	58.9647
		100	-26.4912	6.3150	-0.1032	-0.1093	-1.7023	0.3917	-0.5070	58.9644
	3D solution	Dumir et al. (1997)	-26.4865	6.3387	-0.1026	-0.1087	-1.5189	0.3982	-0.5070	58.9644
		3D solution								
		Dumir et al. (1997)	-26.49	6.340	-0.1024	-0.1086	-1.410	0.3984	-0.5070	58.96
		3D solution								
		Wu and Syu (2007)	-26.4863	-6.3397	-0.1024	-0.1086	-1.4705	0.3984	-0.5070	58.9643
100	Present solution NL = 4	6	-26.1898	1.8982	-0.1000	-0.1008	-10.0306	-1.2139	-0.5012	59.9192
		8	-26.0788	2.2453	-0.0999	-0.1007	-7.7963	-0.3204	-0.5012	59.9193
		10	-26.0399	2.3668	-0.0998	-0.1007	-6.4397	-0.0070	-0.5012	59.9193
		20	-26.0219	2.4231	-0.0997	-0.1007	-5.5490	0.1378	-0.5012	59.9193
		100	-25.9979	2.4981	-0.0997	-0.1006	-3.5951	0.3310	-0.5012	59.9193
	3D solution	Dumir et al. (1997)	-25.9902	2.5221	-0.0996	-0.1005	-1.8661	0.3928	-0.5012	59.9193
		3D solution								
		Dumir et al. (1997)	-25.99	2.523	-0.0996	-0.1005	-1.411	0.3953	-0.5012	59.92
		3D solution								
		Wu and Syu (2007)	-25.9899	2.5231	-0.0996	-0.1005	-1.4108	0.3953	-0.5012	59.9193

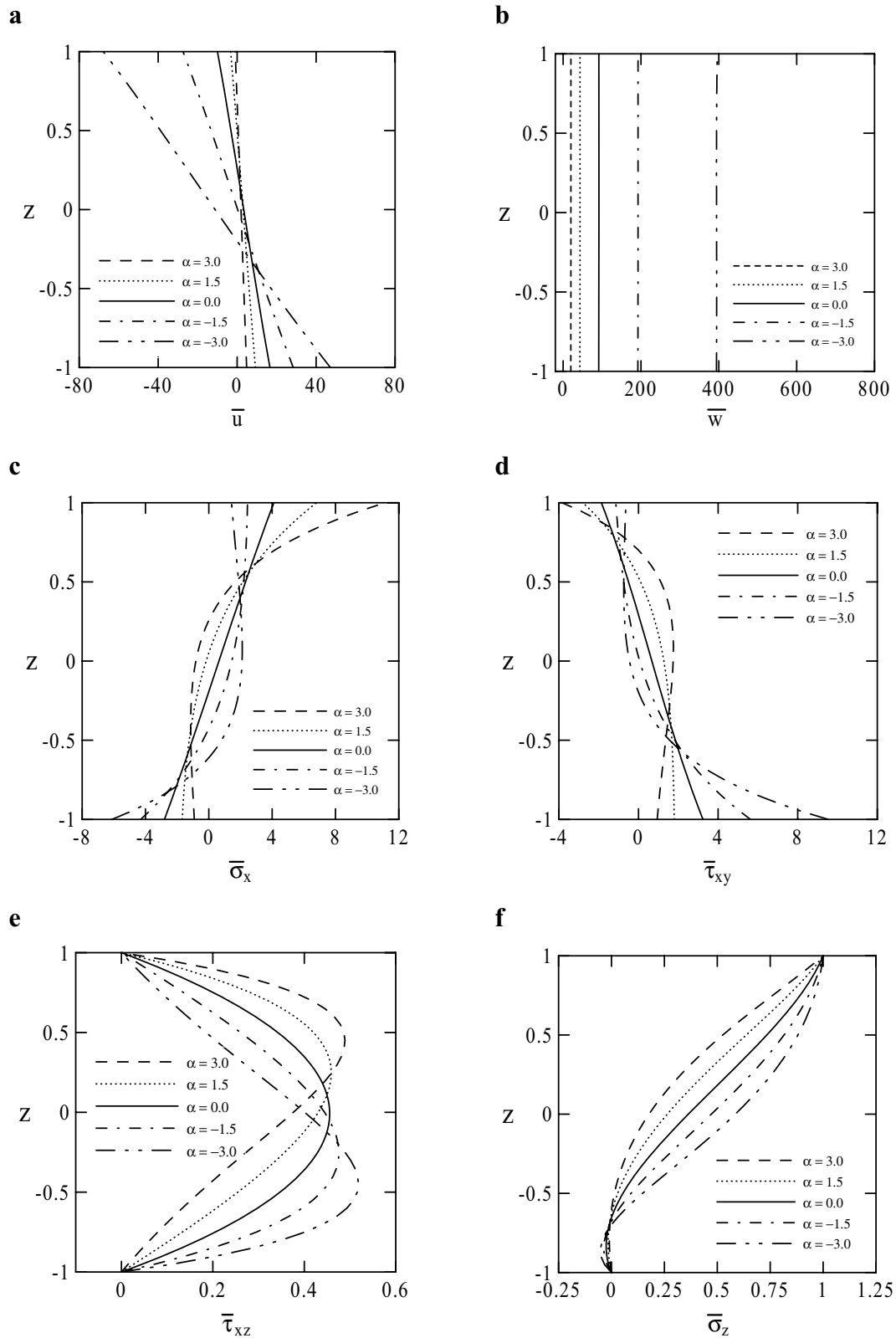


Figure 2: Influence of the material property gradient index on the through-the-thickness distributions of elastic field variables of FG elastic shells under mechanical load (Case 1).

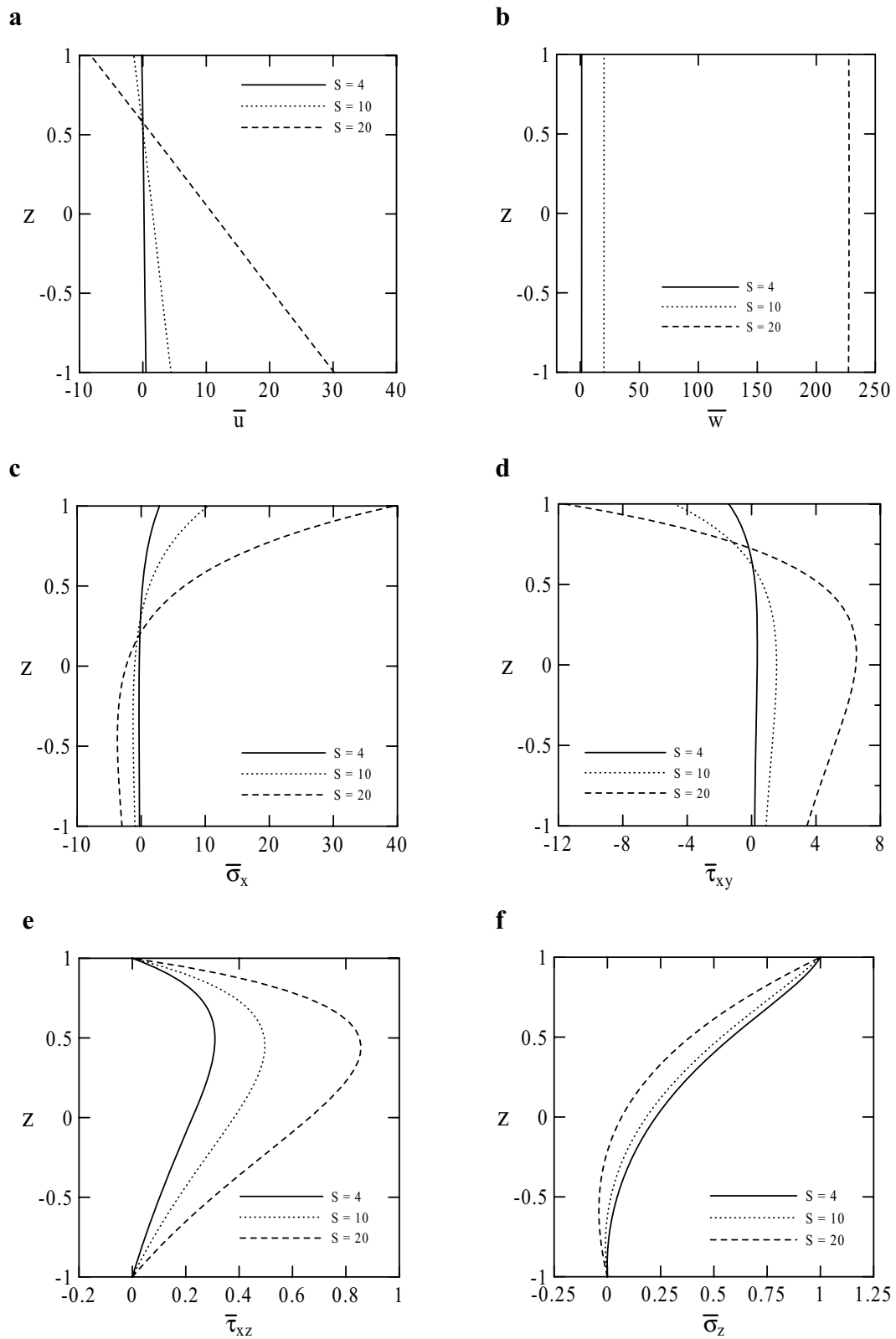


Figure 3: Influence of the span-to-thickness ratio on the through-the-thickness distributions of elastic field variables of FG elastic shells under mechanical load (Case 1).

The influence of the material property gradient index on the through-the-thickness distributions of various elastic field variables is presented in Fig. 2. The geometric parameters are considered as $R_\alpha/a_\alpha=5$, $R_\beta/a_\beta=10$, $a_\alpha/a_\beta=1$ and $a_\alpha/2h=10$; the material property gradient index is taken as $\alpha=3.0, 1.5, 0.0, -1.5$ and -3.0 . It is shown that the through-the-thickness distributions of in-surface stresses is linear for the single-layer homogeneous elastic shell ($\alpha=0$) and the higher-order polynomial variations for the FG shells ($\alpha \neq 0$). The distributions of transverse shear stress are the higher-order polynomial variations through the thickness of the shell. The maximum value of the transverse shear stress occurs at the middle surface in the case of single-layer homogeneous elastic shell ($\alpha=0$). The position of maximum value of transverse shear stress is moving toward the upper surface as α is positive ($\alpha > 0$) and increases; whereas it is moving toward the lower surface as α is negative ($\alpha < 0$) and decreases.

The influence of the span-to-thickness ratio on the through-the-thickness distributions of various field variables are given in Fig. 3. The geometric parameters and material property gradient index are considered as $R_\alpha/a_\alpha=10$, $R_\beta/a_\beta=10$, $a_\alpha/a_\beta=1$, $S = a_\alpha/2h=4, 10, 20$ and $\alpha=3.0$, respectively. It is shown that the in-surface stresses and transverse shear produced in the thin shells ($S=20$) are much larger than those in the thick shells ($S=4$).

5.4 FG Piezoelectric Shells

The direct and converse piezoelectric effects of FG piezoelectric cylindrical shells under the cylindrical bending type of electro-mechanical loads (Cases 4 and 5) are studied in Figs. 4-5 and Figs. 6-7, respectively. The piezoelectric material of PZT-4 is used as the material of bottom surface and its material properties are given in Table 1. The dimensionless field variables are given as follows:

For loading condition of Case 4 (Eq. (40)),

$$\begin{aligned} (\bar{v}, \bar{w}) &= (u_\beta, u_\zeta)(c^*/2hq_0), \\ (\bar{\sigma}_i, \bar{\tau}_{ij}) &= (\sigma_i, \tau_{ij})/q_0, \\ \bar{\Phi} &= \Phi e^*/q_0(2h), \\ \bar{D}_i &= D_i c^*/q_0 e^*; \end{aligned} \quad (48)$$

For loading condition of Case 5 (Eq. (41)),

$$\begin{aligned} (\bar{v}, \bar{w}) &= (u_\beta, u_\zeta)(e^*/2hD_0), \\ (\bar{\sigma}_i, \bar{\tau}_{ij}) &= (\sigma_i, \tau_{ij})(e^*/D_0 c^*), \\ \bar{\Phi} &= \Phi (e^*)^2/D_0 c^*(2h), \\ \bar{D}_i &= D_i/D_0; \end{aligned} \quad (49)$$

where $e^* = 10C/m^2$.

The geometric parameters and material property gradient index are taken as $S = a_\beta/2h=10$, $a_\beta/R_\beta = \pi/3$, $\alpha=3.0, 1.5, 0.0, -1.5, -3.0$ in Figs. 4 and 6; $S = a_\beta/2h=4, 10, 100$, $a_\beta/R_\beta = \pi/3$ and $\alpha=3$ in Figs. 5 and 7.

The influence of material property gradient index on the through-the-thickness distributions of various field variables of the moderately thick FG shells ($S=10$) under the applied mechanical load and applied electric displacement is shown in Figs. 4 and 6, respectively. It is shown that the through-the-thickness distributions of electric field variables change dramatically in the cases of applied mechanical load as the index α becomes a negative value; whereas those of transverse stresses change dramatically in the cases of applied electric displacement as the index α becomes a negative value. It is also shown that the distributions of various field variables through the thickness coordinate of the homogeneous shells ($\alpha = 0$) reveal different patterns with those of the FG shells ($\alpha \neq 0$) in the cases of applied electric displacement.

The influence of the span-to-thickness ratio on the through-the-thickness distributions of various field variables of the FG shells ($\alpha=3$) under the applied mechanical load and applied electric displacement is shown in Figs. 5 and 7, respectively. It is shown that the transverse stresses produced in the thick shells ($S=4$) are larger than those in the thin shells ($S=20$) as the shells are under the applied electric displacement; on the contrary, the transverse stresses produced in the thick

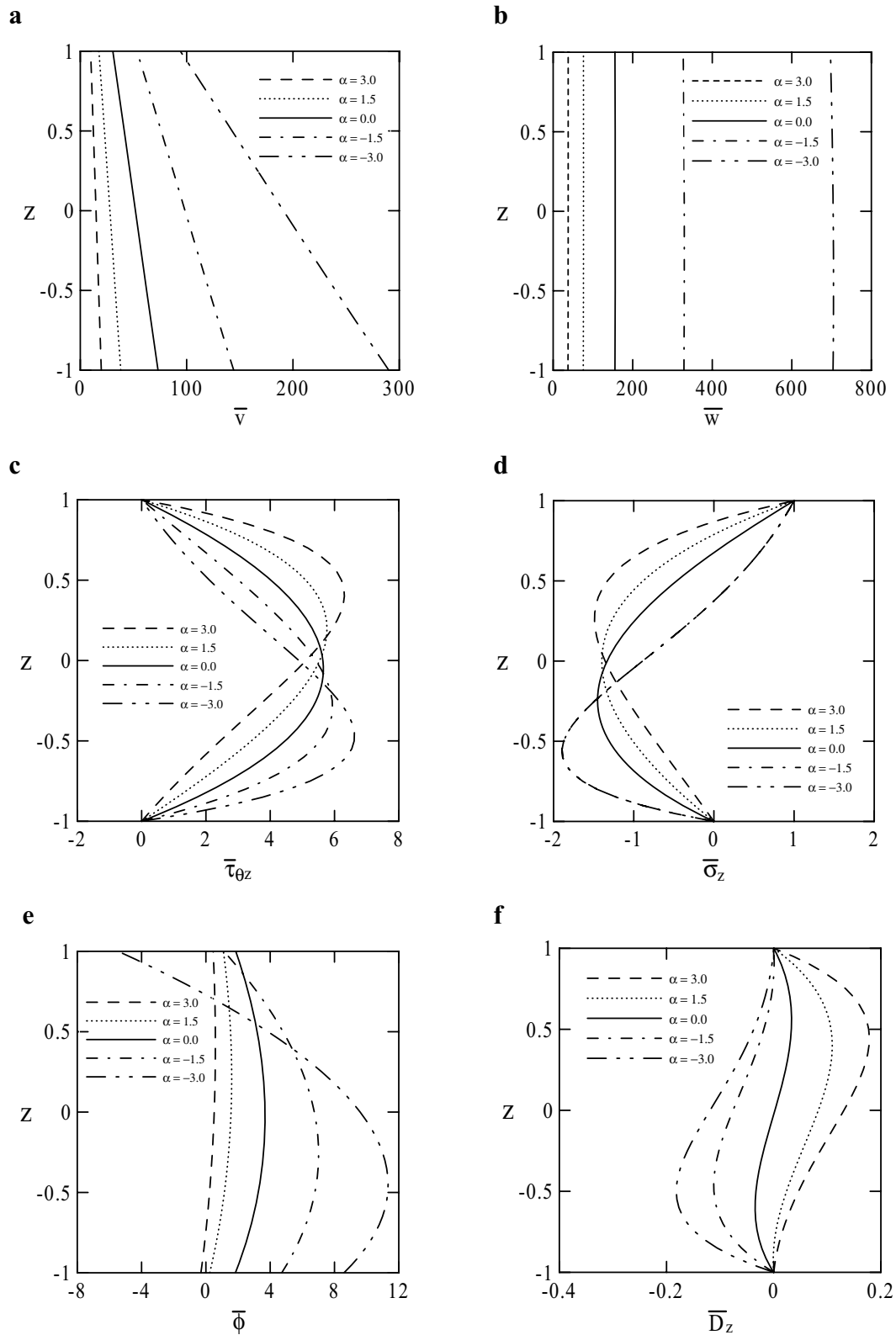


Figure 4: Influence of the material property gradient index on the through-the-thickness distributions of elastic and electric field variables of FG piezoelectric shells under mechanical load (Case 4).

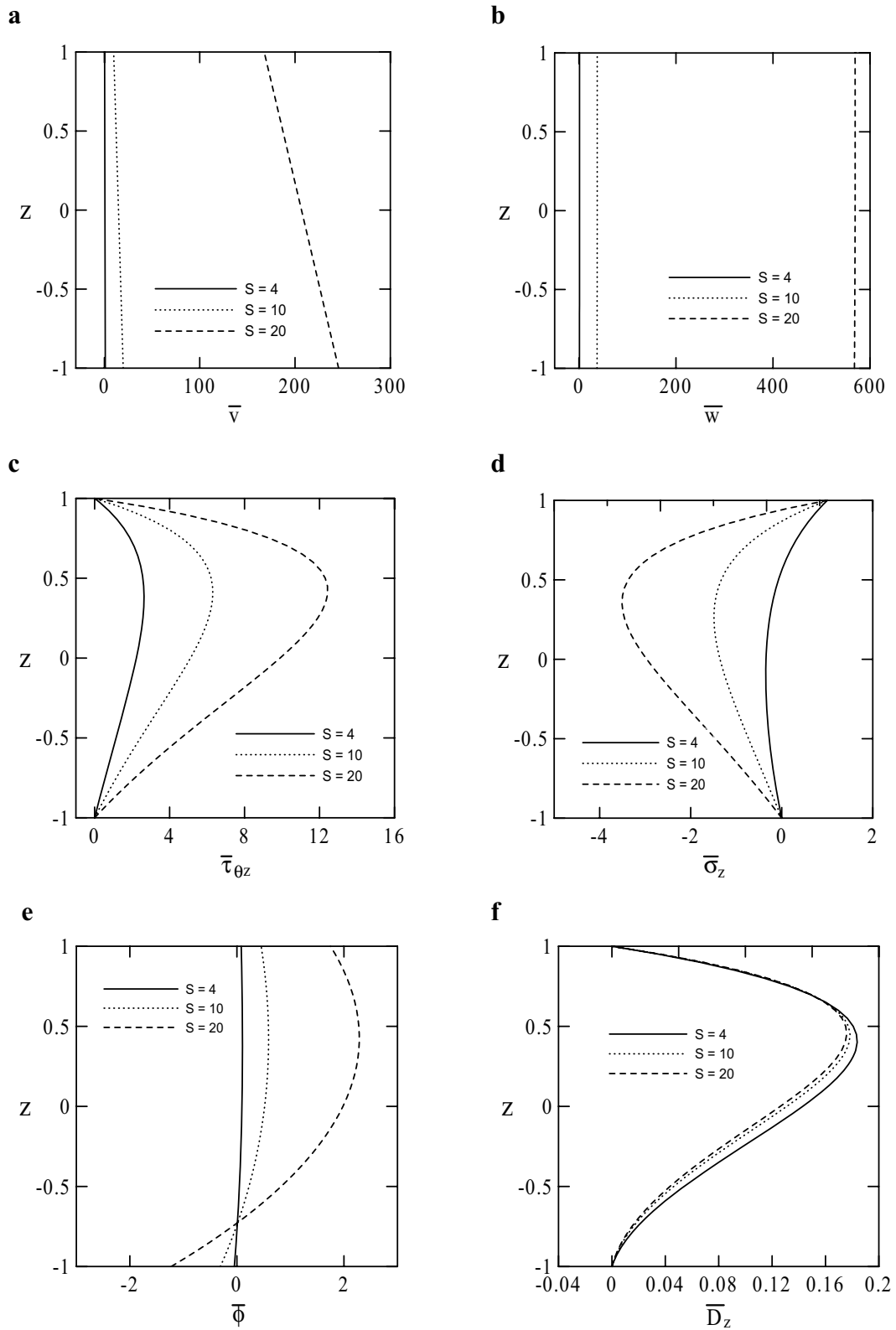


Figure 5: Influence of the span-to-thickness ratio on the through-the-thickness distributions of elastic and electric field variables of FG piezoelectric shells under mechanical load (Case 4).

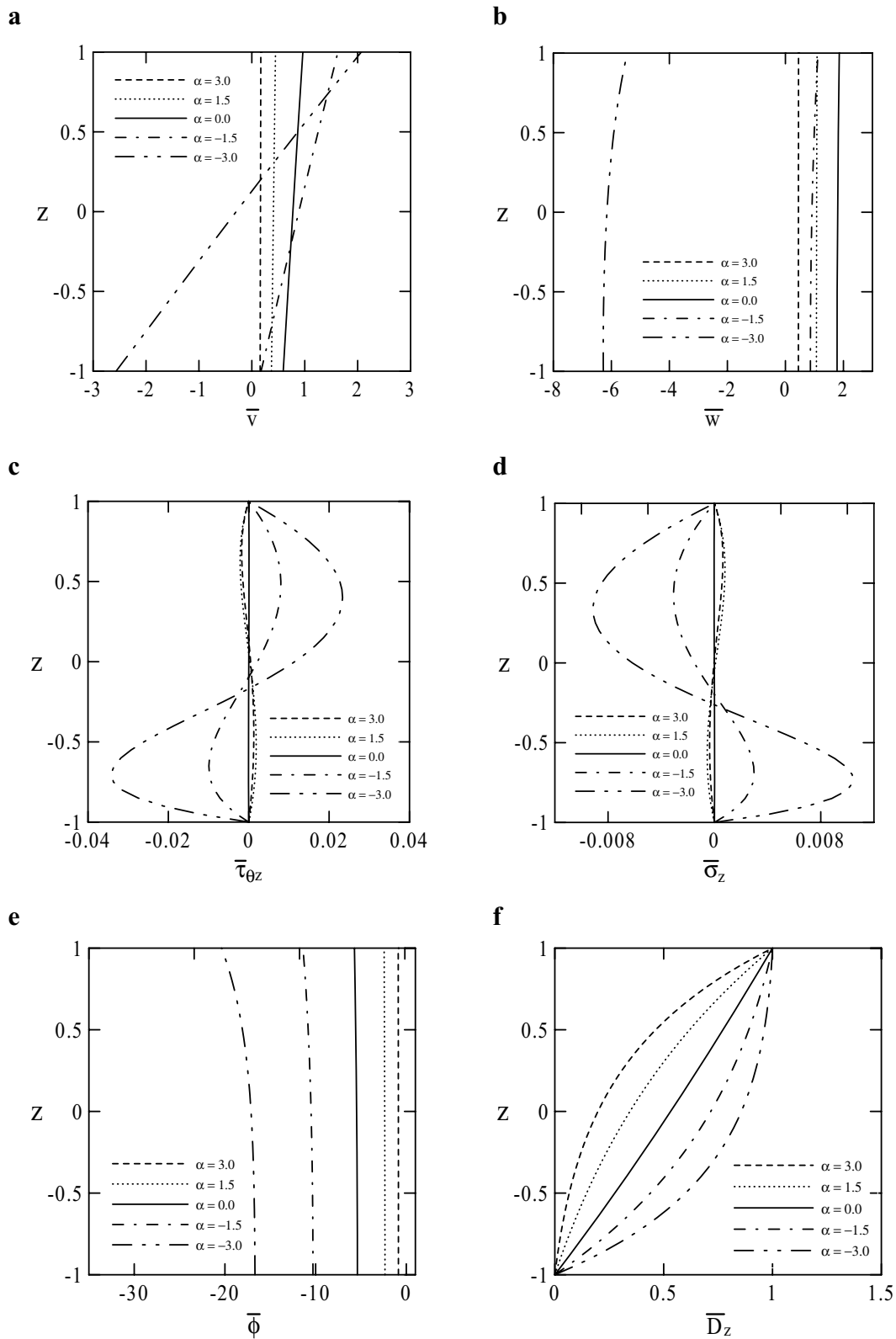


Figure 6: Influence of the material property gradient index on the through-the-thickness distributions of elastic and electric field variables of FG piezoelectric shells under electric displacement (Case 5).

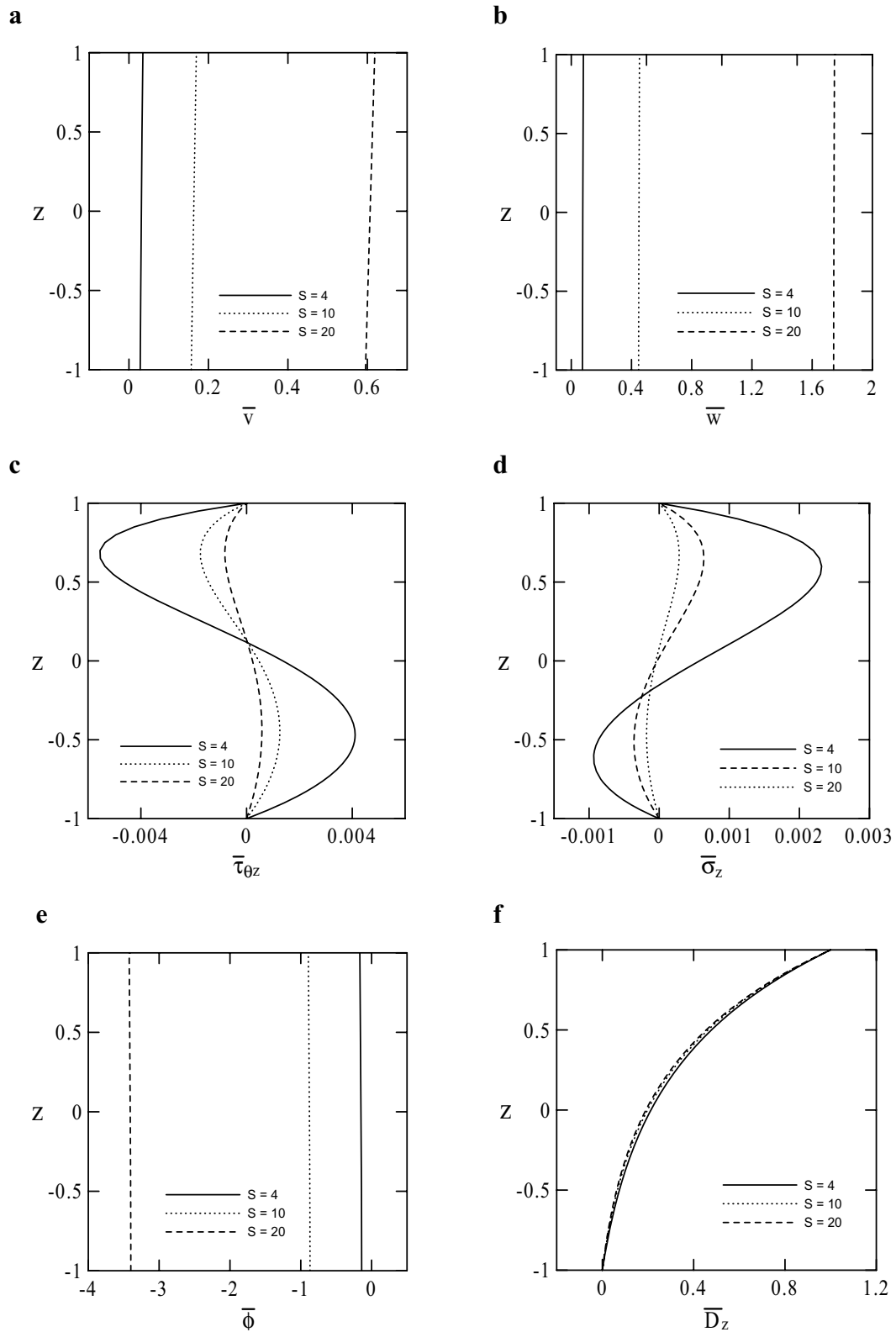


Figure 7: Influence of the span-to-thickness ratio on the through-the-thickness distributions of elastic and electric field variables of FG piezoelectric shells under electric displacement (Case 5).

shells are smaller than those in the thin shells in the cases of applied mechanical load. It is also shown that the influence of the span-to-thickness ratio on the electric displacement is minor, but on other field variables is significant in the cases of the applied mechanical load and applied electric displacement.

6 Concluding remarks

A state space formulation is developed for the static analysis of simply supported, doubly curved functionally graded piezoelectric shells under various electro-mechanical loads. Without loss of generality, the material properties of FG shells are assumed to obey the exponent-law dependence through the thickness coordinate. The present formulation includes the previous state space formulations of single-layer homogeneous, multi-layered and FG piezoelectric plates as well as FG elastic shells as the special cases by letting the curvature radius an infinitely large value and the piezoelectric coefficients zero, respectively. The present state space solutions are validated by making the comparisons with the 3D solutions obtained by both the power series method and the method of perturbation available in the literature. A parametric study for the influences of material property gradient index and the span-to-thickness ratio on the through-the-thickness distributions of various field variables is made. It is noted that the through-the-thickness distributions of various field variables in FG piezoelectric shells reveal different patterns from those in homogenous piezoelectric shells in the cases of applied electric displacement. Based on the previous illustrations, we suggest that an advanced 2D theory may be necessary to be developed for the analysis of FG piezoelectric shells.

Acknowledgement: This work is supported by the National Science Council of Republic of China through Grant NSC 96-2211-E006-265.

References

Bufler, H. (1971): Theory of elasticity of a multilayered medium. *J. Elasticity*, vol. 1, pp. 125-

143.

Chen, W. Q.; Ding, H. J.; Xu, R. Q. (2001): Three-dimensional static analysis of multi-layered piezoelectric hollow spheres via the state space method. *Int. J. Solids Struct.*, vol. 38, pp. 4921-4936.

Dai, K. Y.; Liu, G. R.; Lim, K. M.; Han, X.; Du, S. Y. (2004): A meshfree radial point interpolation method for analysis of functionally graded material (FGM) plates. *Comput. Mech.*, vol. 34, pp. 213-223.

Dai, K. Y.; Liu, G. R.; Han, X.; Lim, K. M. (2005): Thermomechanical analysis of functional graded material (FGM) plates using element-free Galerkin method. *Comput. Struct.*, vol. 83, pp. 1487-1502.

Dumir, P. C.; Dube, G. P.; Kapuria, S. (1997): Exact piezoelectric solution of simply-supported orthotropic circular cylindrical panel in cylindrical bending. *Int. J. Solids Struct.*, vol. 34, pp. 685-702.

Fan, J. R.; Ye, J. Q. (1990): Exact solutions for axisymmetric vibration of laminated circular plate. *J. Engrg. Mech. ASCE*, vol. 116, pp. 920-927.

Fan, J. R.; Zhang, J. (1992): Analytical solutions for thick doubly curved laminated shells. *J. Engrg. Mech. ASCE*, vol. 118, pp. 1338-1356.

Ferreira, A. J. M.; Batra, R. C.; Roque, C. M. C.; Qian, L. F.; Martins, P. A. L. S. (2005): Static analysis of functionally graded plates using third-order shear deformation theory and a meshless method. *Compos. Struct.*, vol. 69, pp. 449-457.

Ferreira, A. J. M.; Batra, R. C.; Roque, C. M. C.; Qian, L. F.; Jorge, R. M. N. (2006): Natural frequencies of functionally graded plates by a meshless method. *Compos. Struct.*, vol. 75, pp. 593-600.

Gopinathan, S. V.; Varadan, V. V.; Varadan, V. K. (2000): A review and critique of theories for piezoelectric laminates. *Smart Mater. Struct.*, vol. 9, pp. 24-48.

Han, F.; Pan, E.; Roy, A.K.; Yue, Z.Q. (2006): Responses of piezoelectric, transversely isotropic,

functionally graded, and multilayered half spaces to uniform circular surface loadings. *CMES: Computer Modeling in Engineering & Sciences*, vol. 14, 15-29.

Heyliger, P. (1997): Exact solutions for simply supported laminated piezoelectric plates. *J. Appl. Mech.*, vol. 64, pp. 299-306.

Heyliger, P.; Brooks, S. (1996): Exact solutions for laminated piezoelectric plates in cylindrical bending. *J. Appl. Mech.*, vol. 63, pp. 903-910.

Kapuria, S.; Achary, G. G. S. (2005): Exact 3D piezoelectricity solution of hybrid cross-ply plates with damping under harmonic electro-mechanical loads. *J. Sound Vibr.*, vol. 282, pp. 617-634.

Lee, J. S.; Jiang, L. Z. (1996): Exact electro-elastic analysis of piezoelectric laminae via state space approach. *Int. J. Solids Struct.*, vol. 13, pp. 977-990.

Pan, E. (2003): Exact solution for functionally graded anisotropic elastic composite laminates. *J. Compos. Mater.*, vol. 37, pp. 1903-1920.

Pan, E.; Han, F. (2005): Exact solution for functionally graded and layered magneto-electro-elastic plates. *Int. J. Eng. Sci.*, vol. 43, pp. 321-339.

Ramirez, F.; Heyliger, P. R.; Pan, E. (2006): Static analysis of functionally graded elastic anisotropic plates using a discrete layer approach. *Compos. Part B*, vol. 37, pp. 10-20.

Ren, J. G. (1989): Analysis of simply supported laminated circular cylindrical shell roofs. *Compos. Struct.*, vol. 11, pp. 277-292.

Rogers, T. G.; Watson, P.; Spencer, A. J. M. (1992): An exact three-dimensional solution for normal loading of inhomogeneous and laminated anisotropic elastic plates of moderate thickness. *Proceedings of Royal Society*, vol. A437, pp. 199-213.

Rogers, T. G.; Watson, P.; Spencer, A. J. M. (1995): Exact three-dimensional elasticity solutions for bending of thick inhomogeneous and laminated strips under normal pressure. *Int. J. Solids Struct.*, vol. 32, pp. 1659-1673.

Saravanos, D. A.; Heyliger, P. R. (1999): Mechanics and computational models for laminated

piezoelectric beams, plates, and shells. *Appl. Mech. Rev.*, vol. 52, pp. 305-319.

Sladek, J.; Sladek, V.; Zhang, C.; Garcia-Sanche, F.; Wunsche, M. (2006): Meshless local Petrov-Galerkin method for plane piezoelectricity. *CMC: Comput. Mater. and Continua*, vol. 4, pp. 109-117.

Soldatos, K.P.; Hadjigeorgiou, V.P. (1990): Three-dimensional solution of the free vibration problem of homogeneous isotropic cylindrical shells and panels. *J. Sound and Vibr.*, vol. 137, pp. 369-384.

Srinivas, S.; Rao, A. K. (1970): Bending, vibration and buckling of simply supported thick orthotropic rectangular plates and laminates. *Int. J. Solids Struct.*, vol. 6, pp. 1463-1481.

Vlasov, V. Z. (1957): The method of initial functions in problems of theory of thick plates and shells. in *Proc. Ninth Int. Congress Appl. Mech.*, Brussels, pp. 321-330.

Wang, J.; Liew, K. M.; Tan, M. J.; Rajendran, S. (2002): Analysis of rectangular laminated composite plates via FSDT meshless method. *Int. J. Mech. Sci.*, vol.44, pp.1275-1293.

Wu, C. P.; Chi, Y. W. (2005): Three-dimensional nonlinear analysis of laminated cylindrical shells under cylindrical bending. *Euro. J. Mech. A/Solids*, vol.24, 837-856.

Wu, C. P.; Chiu, S. J. (2002): Thermally induced dynamic instability of laminated composite conical shells. *Int. J. Solids Struct.*, vol. 39, 3001-3021.

Wu, C. P.; Lo, J. Y. (2006): An asymptotic theory for the dynamic response of laminated piezoelectric shells. *Acta Mech.*, vol. 183, pp. 177-208.

Wu, C. P.; Lo, J. Y.; Chao, J. K. (2005): A three-dimensional asymptotic theory of laminated piezoelectric shells. *CMC: Comput. Mater. and Continua*, vol. 2, pp. 119-137.

Wu, C. P.; Syu, Y. S. (2006): Asymptotic solutions for multilayered piezoelectric cylinders under electromechanical loads. *CMC: Comput. Mater. and Continua*, vol. 4, pp. 87-107.

Wu, C. P.; Syu, Y. S. (2007): Exact solutions of functionally graded piezoelectric shells under

cylindrical bending. *Int. J. Solids Struct.*, vol. 44, pp. 6450-6472.

Wu, C. P.; Syu, Y. S.; Lo, J. Y. (2007): Three-dimensional solutions of multilayered piezoelectric hollow cylinders by an asymptotic approach. *Int. J. Mech. Sci.*, vol. 49, pp. 669-689.

Wu, C. P.; Tarn, J. Q.; Chi, S. M. (1996a): Three-dimensional analysis of doubly curved laminated shells. *J. Engrg. Mech. ASCE*, vol. 122, pp. 391-401.

Wu, C. P.; Tarn, J. Q.; Chi, S. M. (1996b): An asymptotic theory for dynamic response of doubly curved laminated shells. *Int. J. Solids Struct.*, vol. 26, pp. 3813-3841.

Ye, J. (2003): *Laminated composite plates and shells-3D modeling*. Springer, London, UK.

Zhong, Z.; Shang, E. T. (2003): Three-dimensional exact analysis of a simply supported functionally gradient piezoelectric plate. *Int. J. Solids Struct.*, vol. 40, pp. 5335-5352.

Appendix A

The relevant differential operators d_{ij} in Eq. (14) are given as follows:

$$\begin{aligned} d_{11} &= h/RR_x\gamma_\alpha, & d_{15} &= hQ/Rc_{55}, \\ d_{17} &= -(1/\gamma_\alpha)\partial_x, \\ d_{18} &= -(hQ/Re) [(e_{15}/c_{55}\gamma_\alpha)\partial_x], \\ d_{22} &= h/RR_y\gamma_\beta, & d_{26} &= hQ/Rc_{44}, \\ d_{27} &= -(1/\gamma_\beta)\partial_y, \\ d_{28} &= -(hQ/Re) [(e_{24}/c_{44}\gamma_\beta)\partial_y], \\ d_{31} &= [(\tilde{Q}_{11}/R_x\gamma_\alpha^2) + (\tilde{Q}_{21}/R_y\gamma_\alpha\gamma_\beta)] \partial_x, \\ d_{32} &= - [(\tilde{Q}_{12}/R_x\gamma_\alpha\gamma_\beta) + (\tilde{Q}_{22}/R_y\gamma_\beta^2)] \partial_y, \\ d_{33} &= -(h/R\gamma_\alpha\gamma_\beta) \left[(1/R_x) + (1/R_y) + (2hz/RR_xR_y) \right. \\ &\quad \left. - (a_{13}\gamma_\beta/R_x) - (a_{23}\gamma_\alpha/R_y) \right], \\ d_{34} &= (e/QR_x\gamma_\alpha)b_{13} + (e/QR_y\gamma_\beta)b_{23}, \\ d_{37} &= [(\tilde{Q}_{11}/R_x^2\gamma_\alpha^2) + (\tilde{Q}_{12} + \tilde{Q}_{21})/R_xR_y\gamma_\alpha\gamma_\beta \end{aligned}$$

$$+ (\tilde{Q}_{22}/R_y^2\gamma_\beta^2)],$$

$$d_{44} = -(h/R) [(1/R_x\gamma_\alpha) + (1/R_y\gamma_\beta)],$$

$$d_{48} = (hQ/Re^2) \left[(1/\gamma_\alpha^2)(e_{15}^2/c_{55} + \eta_{11})\partial_{xx} \right. \\ \left. + (1/\gamma_\beta^2)(e_{24}^2/c_{44} + \eta_{22})\partial_{yy} \right],$$

$$d_{51} = - [(\tilde{Q}_{11}/\gamma_\alpha^2)\partial_{xx} + (\tilde{Q}_{66}/\gamma_\beta^2)\partial_{yy}],$$

$$d_{52} = - [(\tilde{Q}_{12} + \tilde{Q}_{66})/\gamma_\alpha\gamma_\beta] \partial_{xy},$$

$$d_{53} = -(h/R\gamma_\alpha)a_{13}\partial_x, \quad d_{54} = -(e/Q\gamma_\alpha)b_{13}\partial_x,$$

$$d_{55} = -(h/R\gamma_\alpha\gamma_\beta) \left[(2/R_x) + (1/R_y) \right. \\ \left. + (3hz/RR_xR_y) \right],$$

$$d_{57} = - [(\tilde{Q}_{11}/R_x\gamma_\alpha^2) + (\tilde{Q}_{12}/R_y\gamma_\alpha\gamma_\beta)] \partial_x,$$

$$d_{61} = - [(\tilde{Q}_{21} + \tilde{Q}_{66})/\gamma_\alpha\gamma_\beta] \partial_{xy},$$

$$d_{62} = - [(\tilde{Q}_{66}/\gamma_\alpha^2)\partial_{xx} + (\tilde{Q}_{22}/\gamma_\beta^2)\partial_{yy}],$$

$$d_{63} = -(h/R\gamma_\beta)a_{23}\partial_y,$$

$$d_{64} = -(e/Q\gamma_\beta)b_{23}\partial_y,$$

$$d_{66} = -(h/R\gamma_\alpha\gamma_\beta) \left[(1/R_x) + (2/R_y) \right. \\ \left. + (3hz/RR_xR_y) \right],$$

$$d_{67} = - [(\tilde{Q}_{21}/R_x\gamma_\alpha\gamma_\beta) + (\tilde{Q}_{22}/R_y\gamma_\beta^2)] \partial_y,$$

$$d_{73} = (h^2/R^2) [Q\eta_{33}/(e_{33}^2 + c_{33}\eta_{33})],$$

$$d_{74} = (h/R) [ee_{33}/(e_{33}^2 + c_{33}\eta_{33})],$$

$$d_{77} = -(h/R)(a_{13}/R_x\gamma_\alpha + a_{23}/R_y\gamma_\beta),$$

$$d_{84} = -(e^2/Q) [(c_{33})/(e_{33}^2 + c_{33}\eta_{33})],$$

$$d_{87} = -d_{34},$$

$$\tilde{Q}_{ij} = \frac{Q_{ij}}{Q}, \quad Q_{ij} = c_{ij} - a_{3j}c_{i3} - b_{3j}e_{3i}$$

$$(i, j = 1, 2, 6);$$

$$a_{i3} = \frac{e_{33}e_{3i} + \eta_{33}c_{i3}}{e_{33}^2 + \eta_{33}c_{33}}, \quad b_{i3} = \frac{e_{33}c_{i3} - e_{3i}c_{33}}{e_{33}^2 + \eta_{33}c_{33}}$$

$$(i, j = 1, 2, 6).$$

Appendix B

The relevant differential operators l_{ij} in Eq. (15) are given as follows:

$$\begin{aligned}
l_{15} &= hQ/Rc_{55}, \quad l_{17} = -\partial_x, \\
l_{18} &= -(hQ/Re) [(e_{15}/c_{55})\partial_x], \\
l_{26} &= hQ/Rc_{44}, \quad l_{27} = -\partial_y, \\
l_{28} &= -(hQ/Re) [(e_{24}/c_{44})\partial_y], \\
l_{48} &= (hQ/Re^2) \left[(e_{15}^2/c_{55} + \eta_{11})\partial_{xx} \right. \\
&\quad \left. + (e_{24}^2/c_{44} + \eta_{22})\partial_{yy} \right], \\
l_{51} &= -[\tilde{Q}_{11}\partial_{xx} + \tilde{Q}_{66}\partial_{yy}], \\
l_{52} &= -(\tilde{Q}_{12} + \tilde{Q}_{66})\partial_{xy}, \\
l_{53} &= -(h/R)a_{13}\partial_x, \quad l_{54} = -(e/Q)b_{13}\partial_x, \\
l_{61} &= -(\tilde{Q}_{21} + \tilde{Q}_{66})\partial_{xy}, \\
l_{62} &= -[\tilde{Q}_{66}\partial_{xx} + \tilde{Q}_{22}\partial_{yy}], \\
l_{63} &= -(h/R)a_{23}\partial_y, \quad l_{64} = -(e/Q)b_{23}\partial_y, \\
l_{73} &= (h^2/R^2) [Q\eta_{33}/(e_{33}^2 + c_{33}\eta_{33})], \\
l_{74} &= (h/R) [ee_{33}/(e_{33}^2 + c_{33}\eta_{33})], \\
l_{84} &= -(e^2/Q) [(c_{33})/(e_{33}^2 + c_{33}\eta_{33})].
\end{aligned}$$

Appendix C

The relevant coefficients \tilde{b}_{ij} in Eqs. (21)-(22) are given by

$$\begin{aligned}
\tilde{b}_{11} &= (\tilde{Q}_{11}/\gamma_\alpha)\partial_x, \quad \tilde{b}_{12} = (\tilde{Q}_{12}/\gamma_\beta)\partial_y, \\
\tilde{b}_{21} &= (\tilde{Q}_{21}/\gamma_\alpha)\partial_x, \quad \tilde{b}_{22} = (\tilde{Q}_{22}/\gamma_\beta)\partial_y, \\
\tilde{b}_{31} &= (\tilde{Q}_{66}/\gamma_\beta)\partial_y, \quad \tilde{b}_{32} = (\tilde{Q}_{66}/\gamma_\alpha)\partial_x, \\
\tilde{b}_{13} &= (\tilde{Q}_{11}/\gamma_\alpha R_x) + (\tilde{Q}_{12}/\gamma_\beta R_y), \\
\tilde{b}_{23} &= (\tilde{Q}_{21}/\gamma_\alpha R_x) + (\tilde{Q}_{22}/\gamma_\beta R_y), \quad \tilde{b}_{33} = 0 \\
\tilde{b}_{14} &= (h/R)a_{13}, \quad \tilde{b}_{24} = (h/R)a_{23}, \quad \tilde{b}_{34} = 0, \\
\tilde{b}_{15} &= (e/Q)b_{13}, \quad \tilde{b}_{25} = (e/Q)b_{23}, \quad \tilde{b}_{35} = 0, \\
\tilde{b}_{41} &= (ee_{15}/Qc_{55}), \quad \tilde{b}_{42} = 0, \\
\tilde{b}_{43} &= -(Q/e^2\gamma_\alpha) [(e_{15}^2/c_{55}) + \eta_{11}] \partial_x, \\
\tilde{b}_{51} &= 0, \quad \tilde{b}_{52} = (ee_{24}/Qc_{44}), \\
\tilde{b}_{53} &= -(Q/e^2\gamma_\beta) [(e_{24}^2/c_{44}) + \eta_{22}] \partial_y.
\end{aligned}$$

